Nanomechanical Spectroscopy of 2D Materials

Jan N. Kirchhof[1], Yuefeng Yu[1], Gabriel Antheaume[1], Georgy Gordeev[1], Denis Yagodkin[1], Peter Elliott[2], Sangeeta Sharma[2], Stephanie Reich[1] and Kirill I. Bolotin[1*]*

[1] Department of Physics, Freie Universität Berlin, Arnimallee 14, 14195 Berlin, Germany

[2] Max-Born Institute for Nonlinear Optics and Short Pulse Spectroscopy, Max-Born-Strasse 2A, 12489 Berlin Germany

*jan.kirchhof@fu-berlin.de *kirill.bolotin@fu-berlin.de

We introduce a nanomechanical platform for fast and sensitive measurements of the spectrally-resolved optical dielectric function of 2D materials. At the heart of our approach is a suspended 2D material integrated into a high Q silicon nitride nanomechanical resonator illuminated by a wavelength-tunable laser source. From the heating-related frequency shift of the resonator as well as its optical reflection measured as a function of photon energy, we obtain the real and imaginary parts of the dielectric function. Our measurements are unaffected by substrate-related screening and do not require any assumptions on the underling optical constants. This fast ($\tau_{rise} \sim 135\ ns$), sensitive (noise-equivalent power = $90\frac{pW}{\sqrt{Hz}}$), and broadband (1.2 – 3.1 eV, extendable to UV – THz) method provides an attractive alternative to spectroscopic or ellipsometric characterization techniques.

INTRODUCTION

The interaction of light with a solid is encoded in the material's dielectric function $\epsilon_r(\omega) = \epsilon_1(\omega) + i\epsilon_2(\omega)$. Real and imaginary components ϵ_1, ϵ_2 contain the information regarding light absorption, propagation velocity, excitonic and plasmonic resonances, bandgaps, and many-body effects. The dielectric function is usually experimentally determined via spectroscopic ellipsometry,[1–4] a combination of reflection and transmission measurements,[5] or from spectrally-resolved reflection contrast (*dR/R*) using Kramers-Kronig relations.[6–8] Despite the broad applicability of these techniques, they are hard or impossible to apply in many situations. For example, optical measurements under oblique angles as required by spectroscopic ellipsometry are challenging at low temperature, ultra-high vacuum environments, and/or high magnetic fields. Measurements of transmission require large and thin samples on transparent substrates and may be affected by scattering. The Kramers-Kronig analysis requires broadband measurements of reflection and depends on empirical models of optical constants.[9]

For 2D materials, these problems become more severe. On one hand, 2D materials, in particular from the group of transition metal dichalcogenides (TMDs), feature a remarkable zoo of correlated phases including excitonic insulators,[10] Wigner crystals,[11,12] Bose Einstein condensates[13–15] and superconductors.[15] All these phenomena can be studied by analyzing the dielectric function. On the other hand, their observation requires uniform high-quality samples. Such samples are usually encapsulated in hexagonal boron nitride and have sizes in the micron range. Transmission or ellipsometry measurements of such nanostructures at ultralow temperatures or high magnetic fields are challenging.[16] Especially for studying plasmons or polaritons in patterned 2D materials in the form of photonic[17,18] or phononic crystals,[19] new optical characterization methods are needed. In addition, excitations in 2D materials are strongly screened by the underlying substrate. This screening perturbs the dielectric function also affecting the Kramers-Kronig analysis.

Here, we introduce nanomechanical spectroscopy (NMSpec) to accurately and quickly determine the optical dielectric function of 2D materials. For our proof-of principle experiments, we focus on few-layered TMDs, well-understood materials with many pronounced features in their optical response. Our approach employs a suspended membrane made from the 2D material of interest. The mechanical

resonance frequency of that membrane depends on its temperature, which, in turn, depends on the amount light absorbed by the material upon illumination. Therefore, by measuring changes of the resonance frequency of the membrane vs. the energy of photons ($E_\gamma = \hbar\omega$), we determine the absorption of the material. The membrane functions as its own photodetector – only sensitive to the amount of absorbed light and not, for example, to scattering and other losses. By combining the mechanically measured absorption with optically-recorded reflection, we restore the full dielectric function of the 2D material. We achieve very fast ($\tau_{\text{rise}} \sim 135\, ns$) and sensitive (noise-equivalent power = $90 \frac{pW}{\sqrt{Hz}}$) measurements of the dielectric function for TMD materials in the range 1.2 – 3.1 eV. Our approach uses suspended samples – and therefore is unaffected by screening and works for nanostructures. Furthermore, NMSpec does not require complex transmission measurements and therefore should function at low temperatures and high magnetic fields. Finally, by using the 2D materials itself for the detection of absorbed light, we can potentially obtain access to a broad spectral range from THz to UV allowing to study a large variety of materials.

RESULTS

Device design: TMD-SiN hybrid resonators

Our first goal is to design a TMD-based resonator that controllably changes its frequency as it absorbs light. Such a resonator should have predictable mechanical resonances (the fundamental mode at frequency f) with small linewidth (f_{FWHM}) and thus high quality factor ($Q = \frac{f}{f_{\text{FWHM}}}$), linear mechanical response to illumination power, as well as high motion amplitude. To accomplish these goals, we design a hybrid resonator consisting of a TMD suspended over a circular hole in a high quality silicon nitride (SiN) membrane covered with a thin layer of gold. Our finite element method (FEM) simulations show, that the fundamental mode of such a resonator involves the TMD and suspended SiN oscillating together (Fig. 1a).[20,21] Absorption of light by the suspended TMD causes thermal expansion leading to a reduced tension σ_0 in the material and hence softening the resonance frequency of the entire system. Such a design presents several advantages:

First, the device features resonances with high quality factor at room temperature ($Q > 4000$). This is due to the mechanical quality and low losses in SiN and allows us to resolve frequency shifts with high resolution. This is contrast to 2D material-only resonators that show mechanical resonance frequencies with low quality factors (Q~100).[22–25] Second, our design overcomes the disturbance typically associated with optical probing of mechanical resonances. To probe mechanical motion of our devices, we focus the probing beam on the suspended SiN area thereby avoiding heating of the material being measured. Third, in our system the mechanical resonances and their tuning are highly predictable, with device-to-device variations of ~5% or less. This allows us to simulate our systems with high confidence. The uniformity is also interesting from a technological point of view, as it can potentially allow coupling the oscillator to an external system, e.g. an LC-resonator for electrical signal amplification. Again, this is contrast to 2D material-only resonators that are affected by wrinkling and surface contaminations resulting in a large spread of mechanical resonance frequencies and unpredictable tuning.[25–27] Finally, by covering the SiN area with a thin layer of gold (also used for electrical actuation), we increase its reflectivity and thus enhance the signal to noise ratio. We note that the additional weight of the gold layer and high stiffness of SiN reduce the response of the hybrid mode to laser heating. We thus use micromechanical modelling to design a system giving a good compromise between signal strength and sufficient responsivity (Supplementary Fig. 2b,c), resulting in a device with a circular suspended TMD area of 10 μm diameter and a 20 μm square SiN window of 20 nm thickness.

Device fabrication and interferometric motion detection

We realize the design described above by transferring a multilayer TMD (3 and 4 layers) onto a circular hole in a square SiN window covered with gold (see Methods). The mechanical motion of the hybrid SiN-TMD mode is excited by applying an AC+DC voltage between the device and a non-reflective gate ~40 μm below. The motion of the hybrid mode is detected interferometrically (Fig. 1c).[20] Critically, the probe beam (red beam in Fig. 1c) is focused onto the SiN area and does not significantly heat the device. A second laser source of tunable photon energy between 1.2 and 3.1 eV (blue beam in Fig. 1c) is focused on the suspended TMD area. The absorption of light from that beam increases the temperature of the device and downshifts the mechanical resonance, which we detect. All measurements are carried out in

vacuum and at room temperature but are easily extendable to low temperatures and fiber-based setups. Fig. 1d shows the resonance response of the WSe_2 trilayer sample (device #1) without optical excitation. We find a prominent fundamental mode at $f_0 = 4.6702$ MHz with a Q~4500 and multiple higher order modes. We visualize the shape of the fundamental mode by scanning the probe laser across the device and plot the motion amplitude vs. position (Fig 1e, blue). The mode is well described by our simulations (Fig. 1a.) that give its shape (Fig. 1e, red) and frequency ($f_{0,sim}$= 4.770 MHz), confirming the well-controlled nature of our devices.

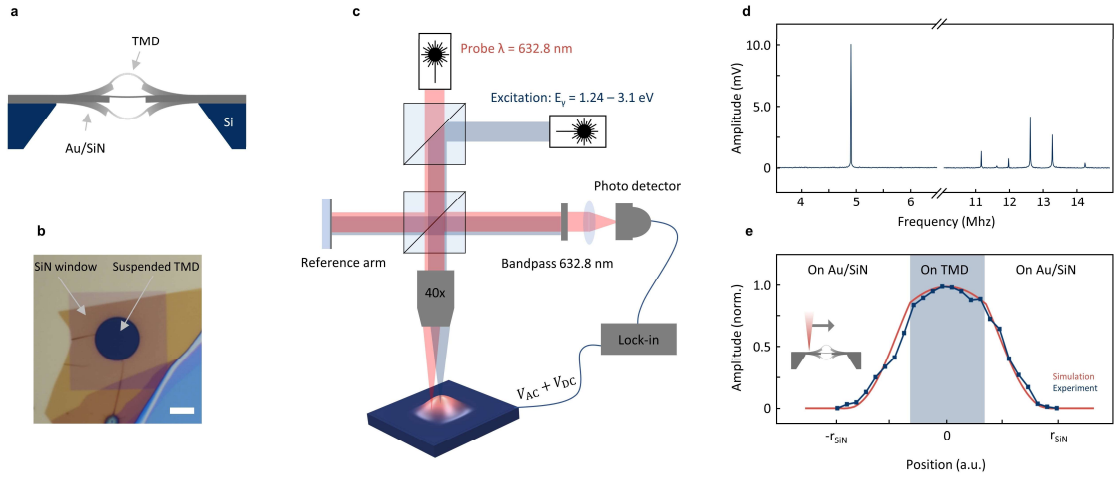

Figure 1. SiN-TMD hybrid devices and interferometric motion detection. a, Sketch of SiN-TMD hybrid resonance mode. The suspended SiN moves together with the TMD material and allows probing the resonances without focusing the probe laser on the TMD area. **b**, Optical micrograph of a WSe_2 trilayer flake suspended on a hole in a SiN window. **c**, Interferometric motion detection using a Michelson interferometer (red laser) with an additional broadly tunable laser (blue) to heat the TMD. The sample is placed in vacuum and the motion of the suspended area is actuated electrically. **d**, Measured amplitude vs. frequency for the trilayer WSe_2 SiN-hybrid device. The fundamental mode shows a large amplitude and enhanced quality factor. **e,** Relative motion amplitude of the fundamental mode extracted along a spatial line scan over the suspended area (blue) in comparison to simulation results (red). The amplitude of motion increases as the probe laser spot moves towards the center of the device and matches the simulated mode shape.

Nanomechanical absorption measurements

Our goal is to use our nanomechanical system to obtain a broadband absorption spectrum of the TMD. To this end we continuously vary the photon energy of the excitation laser and record the resonance response of the high Q fundamental mode. In Fig. 3a we show the raw data of this measurement for the trilayer WSe_2 sample (device #1). Small laser powers ($P < 10$ μW) are sufficient to cause clearly resolvable frequency shifts $\Delta f = f_0 - f$. The resonance frequency softens upon illumination, because

the absorbed light heats the suspended TMD and reduces the built-in tension σ_0. From lower to higher energy, we observe an increasing down shift – in line with an overall increasing absorption towards the band gap of WSe_2. Within the spectra, there are multiple peaks and dips visible. Some of these features (e.g. the dip at 2.96 eV and the sudden jump at 1.91 eV) stem from variations in power of our excitation laser. We record the laser power at the sample position (Supplementary Fig. 5b) and use it to determine the resulting responsivity $\frac{\Delta f}{\Delta P}$ (Fig. 2b). As we show later, the measured responsivity is directly proportional to the optical absorption of the material and the distinct features associated with band-edge excitons of the TMD material are clearly noticeable. We identify the following excitonic transitions: A at 1.63 eV, B at 2.08 eV, A' at 2.28 eV, and B' at 2.68 eV. Positions and widths of theses peaks agree well with literature values.[6,28–30] As a reference, we perform photoluminescence measurements (PL) of the same device (Fig. 2b, grey). As expected, we find the peaks corresponding to A exciton and I exciton, with the latter corresponding to the indirect bandgap of multilayer TMD. For the A exciton, we find an expected small red shift and matching peak width, whereas the indirect peak is not visible in absorption due to the indirect nature of the transition.

Clear peaks are also apparent in the mechanical responsivity data for a second sample made from a different material from the TMD family (4L MoS_2 in Fig. 2c,d). Again, the positions and widths of these peaks match with excitonic transitions dominating optical absorption spectra of MoS_2.[31,32] We note that no assumption regarding material properties has been made in obtaining the spectra in Fig. 2b,d. In all measurements we observe a constant mechanical linewidth around the excitonic peaks (Supplementary Fig. 4a,b) and therefore exclude any cavity or material governed dynamic optomechanical back action effects.[33,34] We note that we can improve the measurement speed and sensitivity further by using a phase-locked loop (PLL) to directly measure the frequency shift vs. photon energy (Supplementary Fig. 5c). We obtain the same frequency response as shown in Fig. 2a, but now we record an entire spectrum in ~3 seconds, only limited by how fast the filter can change the output energy.

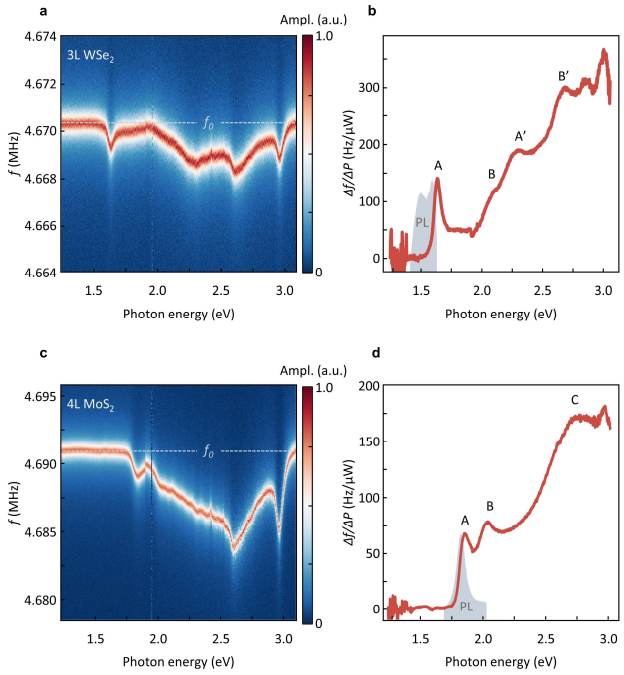

Figure 2. Mechanical absorption spectroscopy in WSe_2 and MoS_2. **a**,**c** Raw frequency response of the TMD-SiN-hybrid device as a function of photon energy for a WSe_2 and a MoS_2 samples. Multiple features are visible and towards higher energies the frequency shift increases as the absorption by the TMD increases. **b**,**d**, Responsivity $\frac{\Delta f}{\Delta P}$ vs. photon energy for WSe_2 and MoS_2. This signal is directly proportion to the absorption and shows clear excitonic features in both samples, which match reference PL measurements (grey). The MoS_2 sample was measured using higher laser power, causing larger absolute frequency shifts.

Optical dielectric function

Next, we determine the optical dielectric function of the TMDs. For this, precise knowledge of both reflection $Refl(E_\gamma)$ and absorption $Abs(E_\gamma)$ in absolute units is required. To convert the measured frequency shift into absorption we model our hybrid system as two springs in series (elastic constants: k_{SiN} and k_{TMD}) and link the responsivity (frequency shift Δf normalized to laser power ΔP) to the energy-depended absorption $Abs(E_\gamma)$ of the TMD via:

$$\frac{\Delta f}{\Delta P}(E_\gamma) = \frac{1}{\sqrt{m_{\mathrm{eff}}}} \frac{\left(\frac{k_{\mathrm{SiN}} k_{\mathrm{TMD}}}{k_{\mathrm{TMD}}+k_{\mathrm{SiN}}}\right)^{\frac{3}{2}}}{2k_{\mathrm{SiN}}} \frac{\beta\, \alpha E_{2\mathrm{D}}}{2h\kappa\sigma_0(1-\nu)} Abs(E_\gamma) \qquad (1)$$

Here m_{eff} is the effective mass of the mode, β is a dimensionless factor determined by the temperature profile in the membrane, α is the thermal expansion coefficient, $E_{2\mathrm{D}}$ is the 2D elastic modulus, κ is the thermal conductivity and ν is the Poisson's ratio of the TMD (full derivation in Supplementary

Information). This expression shows that the responsivity is indeed proportional to the optical absorption. However, in our system, m_{eff} and β can only be obtained numerically and k_{SiN}, k_{TMD} depend on a range of parameters (tension, thermal conductivity etc.) in a complex fashion. We thus use FEM modelling to determine the conversion factor linking $\frac{\Delta f}{\Delta P}(E_\gamma)$ to absorption. We first measure the frequency shift vs. incident laser power for 2.92 (425 nm) and 2.07 eV (600 nm) (Fig. 3a,b). For both energies we observe a linear and reversible downshift of the resonance frequency with increasing laser power (Fig. 3c). Having experimentally confirmed the linear behavior, we use the computed conversion factor (details on mechanical modelling in Supplementary Information) to convert $\frac{\Delta f}{\Delta P}$ to absorption. For the fitted slopes from Fig. 3c (201±14 Hz/μW and 61±11 Hz/μW for 2.92 and 2.07 eV respectively), we get 30.4% and 11.2% absorption by the TMD membrane at respective energies. This is close to expectations.[6,29] The simulation results also allow us to estimate the average temperature increase in the suspended TMD (Fig. 3c, right axis). For 30 μW laser power and 30.4% absorption, we find an increase to only a few degrees above room temperature, which is well inside the linear regime and below the TMD damage threshold.

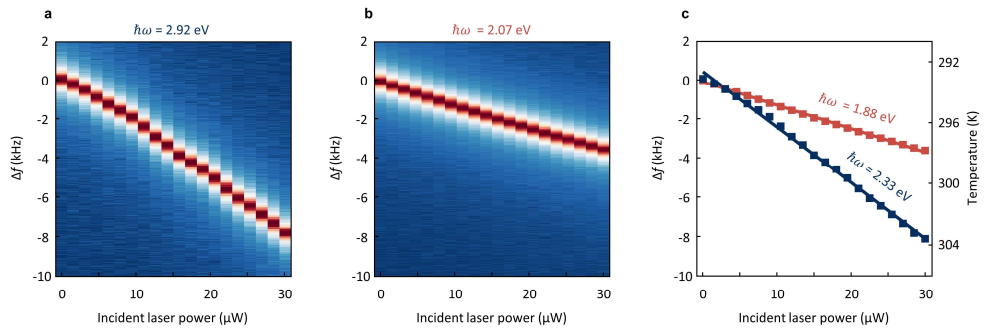

Figure 3. Mechanical response to laser heating. a,b, Frequency shift of the fundamental mode of a suspended trilayer WSe_2 SiN-hybrid device vs. incident laser power for 2.92 and 2.07 eV excitation. A fraction of light absorbed by the membrane causes heating, which reduces the built-in tension and softens the mechanical resonance. **c,** Fits to the frequency change vs. incident laser power, which by comparison to FEM-simulations allows to extract the absorption of the material at different energies. Right axis shows the average temperature in the suspended TMD obtained from such simulations.

Having extracted absorption, we are ready now to evaluate the dielectric function. In Fig. 4a,d we plot the spectrally resolved absorption (*Abs*) data for both samples obtained from the frequency shifts using the conversion factor (red traces). Next, we record reflection (*Refl*) off the TMD in the same

sample configuration and same setup (blue traces in Fig. 4a,d, see method for details). We then use the transfer-matrix approach to relate reflected and absorbed light and obtain the complex refractive index *n* and finally ϵ_1 and ϵ_2 by solving a system of equations at each measured energy (see Methods):

$$\begin{cases} 1 - Abs - Refl = 1/|M_{11}(d, n(\epsilon_1, \epsilon_2))|^2 \\ Refl = |M_{21}(d, n(\epsilon_1, \epsilon_2))|^2 / |M_{11}(d, n(\epsilon_1, \epsilon_2))|^2 \end{cases}$$

Here d is TMD thickness and M_{ij} are the matrix elements corresponding to the reflection and transmission from a thin suspended film (details in SI). No material parameters, except the thickness, are assumed in these formulas. The resulting ϵ_1 and ϵ_2 for 3L WSe_2 and 4L MoS_2 are plotted in Fig. 4b,c,e,f. Both real and imaginary parts of the dielectric function agree well with previous measurements.[1–4,6] Furthermore we find a close agreement with our ab-initio GW-Bethe Salpeter equation (GW-BSE) calculations (shaded in Fig.4b,c,e,f). The difference between measurements and theory for the real part of the dielectric function towards higher energies arises due to the known underestimation of the dielectric function by GW-BSE calculations in this regime. Using NMSpec, we now have obtained full spectroscopic information of the material under test and thereby access to a majority of physical phenomena that make TMDs so exciting.

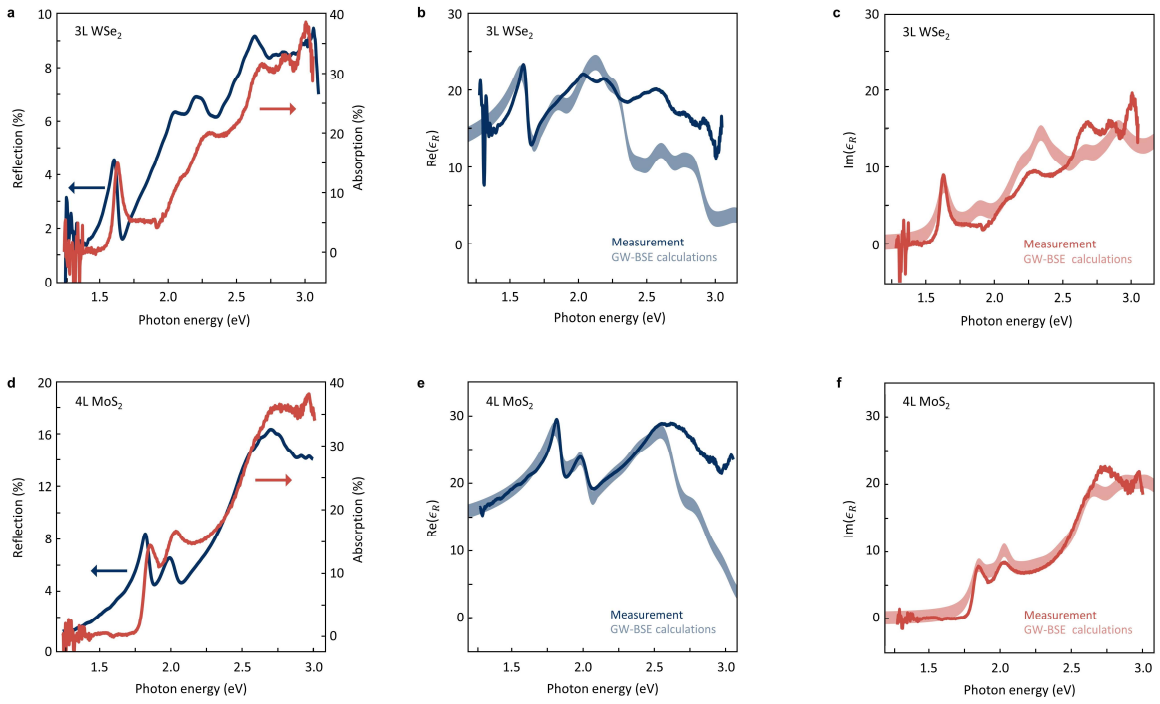

Figure 4. Dielectric function of WSe_2 and MoS_2. a,d Absorption (obtained from NMSPec, red) and reflection (obtained optically, blue) for WSe_2 and MoS_2 vs. photon energy. Similar excitonic features are apparent in both measurements. **b,c,e,f** Real (blue) and imaginary (red) part of the dielectric function of both materials derived from absorption and reflection data (a,d). We find reasonable agreement for GW-BSE calculations (red, blue shaded).

Characterization of the nanomechanical platform

How fast and how sensitive is NMSpec? The measurement speed is ultimately limited by the temperature equilibration time in the suspended TMD. To estimate this parameter, in Fig. 5a we plot the simulated average temperature of the suspended TMD vs. time after turning on the illumination (for a photon energy of 2.92 eV and 30 μW incident laser power). We extract a rise time of $\tau_{\mathrm{rise}} \sim 135\ ns$, which corresponds to a bandwidth of 7.4 MHz, in line with experimental data for TMD devices of similar size.[35] To assess the sensitivity of our system, we determine the noise-equivalent power:

$$\eta = \frac{\sigma_{\mathrm{A}}\sqrt{t} f_0}{\frac{\Delta f}{\Delta P}}, \qquad (2)$$

where $\frac{\Delta f}{\Delta P}$ is the responsivity (determined above), σ_{A} is the Allan deviation obtained from time stability measurements (Fig. 5b,c) and t is the sampling period.[36] For an optimal sampling period of 4 ms, we obtain $\eta = 90\ \frac{pW}{\sqrt{Hz}}$. This is only slightly higher than, for instance, state-of-the-art bolometers (2–100

$\frac{pW}{\sqrt{Hz}}$).[37–40] Nevertheless, the bandwidth is higher by several orders of magnitude for our 2D material-based system, which allows us to measure much faster.

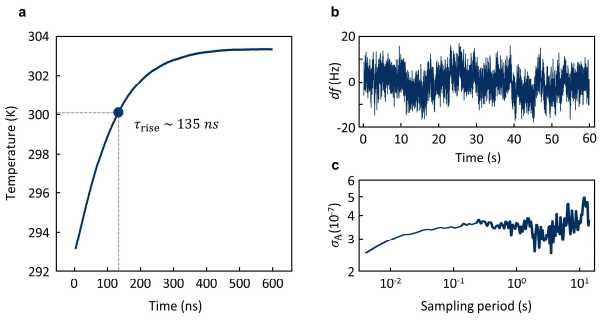

Figure 5. Time resolution and sensitivity a, Simulated time response of the average temperature in the suspended TMD as laser heating is introduced at t = 0 for 2.92 eV (30.4% absorption) and 30 µW laser power. We extract a rise time of 135 ns. **b,** Stability measurement of frequency vs. time without laser illumination, measured using a phase-locked loop. **c)** Extracted Allan deviation σ_A vs. integration time in log-log scale derived from **b)**

Discussion and outlook

Overall, NMSpec is a new approach to obtain the dielectric function of 2D materials. This method is sensitive ($\eta = 90\ \frac{pW}{\sqrt{Hz}}$), fast ($\tau_{\mathrm{rise}} = 135\ ns$), and accurate. The absorption spectrum as well as the dielectric function for WSe_2 and MoS_2 are close to that obtained by others means. The approach does not require complex dielectric modelling or assumption about the material's optical properties (compared to e.g. constrained Kramer-Kronig analysis), optical transmission measurements (that are very difficult e.g. at low temperatures or high magnetic fields),[16] and works for samples the sizes of a diffraction-limited laser spot (unlike e.g. ellipsometry approaches). Moreover, NMSpec directly records optical absorption and is insensitive to scattering that is often hard to discriminate in all-optical techniques. By directly working with suspended samples, our approach is independent of tabulated optical constants of external materials and avoids perturbation of the excitonic features in 2D materials due to screening. Finally, as the material serves as its own detector, it is relatively straightforward to extend the approach to different spectral ranges.

The sensitivity of our approach can be increased much further. First, the quality factor of optimized SiN membranes can reach $Q > 10^8$,[41] compared to around 10^3 used here. This should likely result in a correspondingly higher measurement sensitivity. Second, Eq. 1 shows that the responsivity of NMSpec

is inversely proportional to the thermal conductivity of the 2D material. This quantity can be reduced by e.g. patterning the membrane into a trampoline shape[40] or e.g. via defect-engineering.[42,43] Third, at low temperatures the mechanical quality factor increases while the ratio of thermal conductivity and thermal expansion entering Eq.1 stays roughly constant. Therefore, we expect the low temperature sensitivity of our approach to increase. The combination of 2D materials with low loss SiN results in enhanced Qs and therefore provides an attractive platform for studying optomechanical cooling and self-oscillation phenomena – especially at low temperatures. Finally, we hope to implement our measurement scheme completely on a chip using electrical readout to create a compact, robust, and highly sensitive nanomechanical platform for spectroscopic characterization of 2D materials.

Methods

Fabrication

To fabricate our hybrid devices, we transfer TMDs onto a circular hole using the all-dry PDMS method.[44] The SiN chip is beforehand covered with a thin layer of gold (30 nm) to electrically contact the TMD and to increase its reflectivity. After transfer we perform an annealing step (3 h, 200 °C) in vacuum to remove residues and assure good adhesion to the substrate.

Interferometric detection

The sample is placed upside down in a vacuum chamber of $< 10^{-5}$ mbar. By applying a DC+AC voltage relative to the non-reflective gate electrode, we mechanically actuate the suspended area of the chip. The motion of the TMD is detected by a Michelson interferometer. In this detection scheme we focus a 632.8 nm HeNe laser (<1 μW, ~1.5 μm spot size) on the SiN area of the sample and the reflected light is superimposed with the light coming from the reference arm and guided into an avalanche photodetector. The resulting interference signal is highly sensitive to relative displacements and allows us to detect the motion of suspended samples with high spatial resolution. We actively stabilize the relative position of the reference arm via a mirror on a piezo and thereby ensure constant interference conditions and good signal strength over a large period of time (setup details in Supplementary Fig. 5). In addition to the probe laser, we implement an excitation laser of tunable colour (1.2 – 3.1 eV, blue in Fig. 1c). We use a band pass filter (BP) to block the excitation laser from reaching the detector and overloading it. The large separation (40 μm) of the non-reflective gate and sample negates all cavity-related optomechanical backaction effects (details in Supplementary section 5) and allows us to measure purely static heating effects in our sample over a very large range of photon energies.

FEM simulations

For the finite element modelling we use the structural mechanics of COMSOL Multiphysics (Version 5.5). We build a model around the suspended area partially including the silicon support and use a swept mesh for the thin layers. To determine the resonance frequencies, we use a pre-stressed eigenfrequency study. To include laser heating, we add a study step and calculate the heat profile upon laser heating (Gaussian beam) of the center of the suspended TMD. This then allows us to determine the tuning of the fundamental mode and extract the conversion factor. All parameters and details in supplementary information.

Photoluminescence measurements

Photoluminescence measurements were performed on a Horiba Xplora Raman spectrometer in backscattering configuration using a 100x (NA 0.9) objective and 532 nm excitation. Spectra were acquired using an integration time of 5 s and with a laser power of 4 μW to avoid heating.

Reflection measurements

Reflection measurements are performed in the same setup by blocking the reference arm and the probe laser and then sweeping the tunable light source whilst recording the reflected signal off our sample. Spectra from an empty hole are subtracted and the result are normalized by dividing by a "100% reflection reference", which is obtained by measuring reflection off a silver mirror with known reflection properties. More details in supplementary information.

Acknowledgements

This work was supported by Deutsche Forschungsgemeinschaft (DFG, German Research Foundation, project-ID 449506295 and 328545488), CRC/TRR 227 (project B08 and A04), ERC Starting grant no. 639739 and CSC 202006150013.

References

(1) Liu, H. L.; Shen, C. C.; Su, S. H.; Hsu, C. L.; Li, M. Y.; Li, L. J. Optical Properties of Monolayer Transition Metal Dichalcogenides Probed by Spectroscopic Ellipsometry. *Appl. Phys. Lett.* **2014**, *105* (20), 201905.

(2) Li, W.; Birdwell, A. G.; Amani, M.; Burke, R. A.; Ling, X.; Lee, Y. H.; Liang, X.; Peng, L.; Richter, C. A.; Kong, J.; Gundlach, D. J.; Nguyen, N. V. Broadband Optical Properties of Large-Area Monolayer CVD Molybdenum Disulfide. *Phys. Rev. B - Condens. Matter Mater. Phys.* **2014**, *90* (19).

(3) Yim, C.; O'Brien, M.; McEvoy, N.; Winters, S.; Mirza, I.; Lunney, J. G.; Duesberg, G. S. Investigation of the Optical Properties of MoS2 Thin Films Using Spectroscopic Ellipsometry. *Appl. Phys. Lett.* **2014**, *104* (10), 103114.

(4) Shen, C. C.; Hsu, Y. Te; Li, L. J.; Liu, H. L. Charge Dynamics and Electronic Structures of Monolayer MoS2 Films Grown by Chemical Vapor Deposition. *Appl. Phys. Express* **2013**, *6* (12), 125801.

(5) Hecht, E. *Optics. 4th Edition*; Addison-Wesley, San Francisco, CA, 2002.

(6) Li, Y.; Chernikov, A.; Zhang, X.; Rigosi, A.; Hill, H. M.; Van Der Zande, A. M.; Chenet, D. A.; Shih, E. M.; Hone, J.; Heinz, T. F. Measurement of the Optical Dielectric Function of Monolayer Transition-Metal Dichalcogenides: MoS2, Mo S E2, WS2, and WS E2. *Phys. Rev. B - Condens. Matter Mater. Phys.* **2014**, *90* (20), 205422.

(7) de L. Kronig, R. On the Theory of Dispersion of X-Rays. *J. Opt. Soc. Am.* **1926**, *12* (6), 547.

(8) Kramers, H. A. The Quantum Theory of Dispersion. *Nature*. Nature Publishing Group 1924, pp 310–311.

(9) Kuzmenko, A. B. Kramers–Kronig Constrained Variational Analysis of Optical Spectra. *Rev. Sci. Instrum.* **2005**, *76* (8), 083108.

(10) Ma, L.; Nguyen, P. X.; Wang, Z.; Zeng, Y.; Watanabe, K.; Taniguchi, T.; MacDonald, A. H.; Mak, K. F.; Shan, J. Strongly Correlated Excitonic Insulator in Atomic Double Layers. *Nature* **2021**, *598* (7882), 585–589.

(11) Zhou, Y.; Sung, J.; Brutschea, E.; Esterlis, I.; Wang, Y.; Scuri, G.; Gelly, R. J.; Heo, H.; Taniguchi, T.; Watanabe, K.; Zaránd, G.; Lukin, M. D.; Kim, P.; Demler, E.; Park, H. Bilayer Wigner Crystals in a Transition Metal Dichalcogenide Heterostructure. *Nature* **2021**, *595* (7865), 48–52.

(12) Zarenia, M.; Neilson, D.; Partoens, B.; Peeters, F. M. Wigner Crystallization in Transition Metal Dichalcogenides: A New Approach to Correlation Energy. *Phys. Rev. B* **2017**, *95* (11), 115438.

(13) Wang, Z.; Rhodes, D. A.; Watanabe, K.; Taniguchi, T.; Hone, J. C.; Shan, J.; Mak, K. F. Evidence of High-Temperature Exciton Condensation in Two-Dimensional Atomic Double Layers. *Nature* **2019**, *574* (7776), 76–80.

(14) Tartakovskii, A. Excitons in 2D Heterostructures. *Nature Reviews Physics*. 2020, pp 8–9.

(15) Novoselov, K. S.; Mishchenko, A.; Carvalho, A.; Castro Neto, A. H. 2D Materials and van Der Waals Heterostructures. *Science (80-.).* **2016**, *353* (6298).

(16) Stier, A. V; Wilson, N. P.; Velizhanin, K. A.; Kono, J.; Xu, X.; Crooker, S. A. Magnetooptics of Exciton Rydberg States in a Monolayer Semiconductor. *Phys. Rev. Lett.* **2018**, *120* (5).

(17) Noori, Y. J.; Cao, Y.; Roberts, J.; Woodhead, C.; Bernardo-Gavito, R.; Tovee, P.; Young, R. J. Photonic Crystals for Enhanced Light Extraction from 2D Materials. *ACS Photonics* **2016**, *3* (12), 2515–2520.

(18) Zhang, L.; Gogna, R.; Burg, W.; Tutuc, E.; Deng, H. Photonic-Crystal Exciton-Polaritons in Monolayer Semiconductors. *Nat. Commun.* **2018**, *9* (1), 1–8.

(19) Kirchhof, J. N.; Weinel, K.; Heeg, S.; Deinhart, V.; Kovalchuk, S.; Höflich, K.; Bolotin, K. I. Tunable Graphene Phononic Crystal. *Nano Lett.* **2021**, *21* (5), 2174–2182.

(20) Singh, R.; Nicholl, R. J. T.; Bolotin, K. I.; Ghosh, S. Motion Transduction with Thermo-Mechanically Squeezed Graphene Resonator Modes. *Nano Lett.* **2018**, *18* (11), 6719–6724.

(21) Schwarz, C.; Pigeau, B.; Mercier De Lépinay, L.; Kuhn, A. G.; Kalita, D.; Bendiab, N.; Marty, L.; Bouchiat, V.; Arcizet, O. Deviation from the Normal Mode Expansion

in a Coupled Graphene-Nanomechanical System. *Phys. Rev. Appl.* **2016**, *6* (6), 064021.

(22) Verbiest, G. J.; Kirchhof, J. N.; Sonntag, J.; Goldsche, M.; Khodkov, T.; Stampfer, C. Detecting Ultrasound Vibrations with Graphene Resonators. *Nano Lett.* **2018**, *18* (8), 5132–5137.

(23) Lee, J.; Wang, Z.; He, K.; Shan, J.; Feng, P. X. L. High Frequency MoS2 Nanomechanical Resonators. *ACS Nano* **2013**, *7* (7), 6086–6091.

(24) Ye, F.; Islam, A.; Zhang, T.; Feng, P. X.-L. Ultrawide Frequency Tuning of Atomic Layer van Der Waals Heterostructure Electromechanical Resonators. *Nano Lett.* **2021**, *21* (13), 5508–5515.

(25) Dolleman, R. J.; Lloyd, D.; Bunch, J. S.; Van Der Zant, H. S. J.; Steeneken, P. G. *Transient Thermal Characterization of Suspended Monolayer MoS 2*.

(26) Nicholl, R. J. T.; Conley, H. J.; Lavrik, N. V.; Vlassiouk, I.; Puzyrev, Y. S.; Sreenivas, V. P.; Pantelides, S. T.; Bolotin, K. I. The Effect of Intrinsic Crumpling on the Mechanics of Free-Standing Graphene. *Nat. Commun.* **2015**, *6*, 8789.

(27) Dolleman, R. J.; Houri, S.; Davidovikj, D.; Cartamil-Bueno, S. J.; Blanter, Y. M.; Van Der Zant, H. S. J.; Steeneken, P. G. Optomechanics for Thermal Characterization of Suspended Graphene. *Phys. Rev. B* **2017**, *96* (16).

(28) Aslan, B.; Yule, C.; Yu, Y.; Lee, Y. J.; Heinz, T. F.; Cao, L.; Brongersma, M. L. Excitons in Strained and Suspended Monolayer WSe 2. *2D Mater.* **2022**, *9* (1), 015002.

(29) Aslan, O. B.; Deng, M.; Heinz, T. F. Strain Tuning of Excitons in Monolayer WSe2. *Phys. Rev. B* **2018**, *98* (11), 115308.

(30) Zhao, W.; Ghorannevis, Z.; Chu, L.; Toh, M.; Kloc, C.; Tan, P. H.; Eda, G. Evolution of Electronic Structure in Atomically Thin Sheets of Ws 2 and Wse2. *ACS Nano* **2013**, *7* (1), 791–797.

(31) Splendiani, A.; Sun, L.; Zhang, Y.; Li, T.; Kim, J.; Chim, C. Y.; Galli, G.; Wang, F. Emerging Photoluminescence in Monolayer MoS2. *Nano Lett.* **2010**, *10* (4), 1271–1275.

(32) Castellanos-Gomez, A.; Quereda, J.; Van Der Meulen, H. P.; Agraït, N.; Rubio-Bollinger, G. Spatially Resolved Optical Absorption Spectroscopy of Single- and Few-Layer MoS2 by Hyperspectral Imaging. *Nanotechnology* **2016**, *27* (11).

(33) Barton, R. A.; Storch, I. R.; Adiga, V. P.; Sakakibara, R.; Cipriany, B. R.; Ilic, B.; Wang, S. P.; Ong, P.; McEuen, P. L.; Parpia, J. M.; Craighead, H. G. Photothermal Self-Oscillation and Laser Cooling of Graphene Optomechanical Systems. *Nano Lett.* **2012**, *12* (9), 4681–4686.

(34) Xie, H.; Jiang, S.; Rhodes, D. A.; Hone, J. C.; Shan, J.; Mak, K. F. Tunable Exciton-Optomechanical Coupling in Suspended Monolayer MoSe2. *Nano Lett.* **2021**, *21* (6), 2538–2543.

(35) Dolleman, R. J.; Lloyd, D.; Lee, M.; Scott Bunch, J.; Van Der Zant, H. S. J.; Steeneken, P. G. *Transient Thermal Characterization of Suspended Monolayer MoS2*; 2018; Vol. 2.

(36) Allan, D. W. Statistics of Atomic Frequency Standards. *Proc. IEEE* **1966**, *54* (2), 221–230.

(37) Bolduc, M.; Terroux, M.; Tremblay, B.; Marchese, L.; Savard, E.; Doucet, M.; Oulachgar, H.; Alain, C.; Jerominek, H.; Bergeron, A. Noise-Equivalent Power Characterization of an Uncooled Microbolometer-Based THz Imaging Camera. *Terahertz Physics, Devices, Syst. V Adv. Appl. Ind. Def.* **2011**, *8023*, 80230C.

(38) Yang, H. H.; Rebeiz, G. M. Sub-10-PW/Hz0.5 Uncooled Micro-Bolometer with a Vacuum Micro-Package. *IEEE Trans. Microw. Theory Tech.* **2016**, *64* (7), 2129–2136.

(39) Abdel-Rahman, M.; Al-Khalli, N.; Zia, M. F.; Alduraibi, M.; Ilahi, B.; Awad, E.; Debbar, N. Fabrication and Design of Vanadium Oxide Microbolometer. In *AIP Conference Proceedings*; 2017; Vol. 1809, p 20001.

(40) Blaikie, A.; Miller, D.; Alemán, B. J. A Fast and Sensitive Room-Temperature Graphene Nanomechanical Bolometer. *Nat. Commun.* **2019**, *10* (1).

(41) Ghadimi, A. H.; Fedorov, S. A.; Engelsen, N. J.; Bereyhi, M. J.; Schilling, R.; Wilson, D. J.; Kippenberg, T. J. Elastic Strain Engineering for Ultralow Mechanical Dissipation. *Science (80-.).* **2018**, *360* (6390), 764–768.

(42) Malekpour, H.; Ramnani, P.; Srinivasan, S.; Balasubramanian, G.; Nika, D. L.;

Mulchandani, A.; Lake, R. K.; Balandin, A. A. Thermal Conductivity of Graphene with Defects Induced by Electron Beam Irradiation. *Nanoscale* **2016**, *8* (30), 14608–14616.

(43) Yan, Z.; Yoon, M.; Kumar, S. Influence of Defects and Doping on Phonon Transport Properties of Monolayer MoSe2. *2D Mater.* **2018**, *5* (3), 000000.

(44) Castellanos-Gomez, A.; Buscema, M.; Molenaar, R.; Singh, V.; Janssen, L.; Van Der Zant, H. S. J.; Steele, G. A. Deterministic Transfer of Two-Dimensional Materials by All-Dry Viscoelastic Stamping. *2D Mater.* **2014**, *1* (1), 011002.